Arash KARIMI POUR [1], Ehsan NOROOZINEJAD FARSANGI [2*]

* Corresponding Author, email: ehsan.noroozinejad@westernsydney.edu.au
1. https://orcid.org/0000-0002-8456-4182
2. https://orcid.org/0000-0002-2790-526X

1. Department of Civil Engineering, University of Texas at El Paso (UTEP), Texas, USA
2. Senior Researcher, Urban Transformations Research Centre (UTRC), Western Sydney University, NSW, Australia

Innovative triangular plate elements for enhanced plate bending analyses

Keywords: triangular element, plate benchmark, precise stress, finite element method, variational principle

The performance of triangular elements satisfying either compatibility or incompatibility conditions in the plate bending analyses is of great importance. To achieve highly accurate responses, four elements are formulated for the structural analysis in this study. All of these elements have thirteen nodes with different degree-of-freedom arrangements. Two of them are displacement-based compatible triangular elements, which are named Karimi Pour Compatible Triangular (KCT) and Noroozinejad Compatible Triangular (NCT) elements. Besides, the other two stress-based incompatible triangular elements are also suggested with the names of Karimi Pour Incompatible Triangular (KIT) and Noroozinejad Incompatible Triangular (NIT) elements. In this study, several benchmark problems are solved by using four proposed elements. These structures were previously analyzed by analytical or numerical schemes. Findings clearly indicated the improvement of answers, when various behaviors of the plate bending structures were studied. Additionally, it is concluded that the solution time is considerably declined if the recommended stress-based elements are utilized.

1. Introduction

The finite element approach consists of several elements that may be used to address a wide range of issues. Displacement techniques are one of the most prevalent methods for creating a new element. The flaw in this technique is that it frequently results in incorrect stresses. There are numerous options for correcting this flaw and improving replies. [1-9]. In this regard, Öztorun [10] presented a new rectangular element for elastic plate-bending bodies. The proposed element had six degrees of freedom. Both numerical and experimental tests were utilized to show the accuracy of the element. Suitable outcomes were achieved using coarse meshes, and rational convergence was also driven for the evaluated benchmarks.

In 2013, Esen [11] defined a new element for solving thin plates under a vibration condition. The matrix of the stiffness of the recommended element was improved using the transverse inertia and Coriolis forces. In this research, a sixteen-degrees-of-freedom rectangular element was presented. The obtained results demonstrated the elemental performance improved in predicting the displacement responses of the plate bending problems. In another investigation, Haldar and Sheikh [12] evaluated the performance of plates using a new finite element formulation. In their proposed element, the impact of shear deformation was considered. Solving different problems demonstrated the acceptable performance of the industrialized element. To solve the plate bending approaches, Wang and Wang [13] utilized finite element schemes for several loading conditions. Governing formulas were established using the Galerkin scheme. To validate their proposed elements, different problems were solved. They declared that the deformation and stress components of the plate element have a theatrical requirement on the structural outstanding surface stress. Moreover, the developed element could be utilized as a useful tool to predict the plate performances.

In 2011, Flores and Oñate [14] presented novel triangular elements to assess the bending behavior of thin membranes and shells. A new integration method was also employed. Besides, all findings were compared with the other previously available answers. Based on the obtained results, the proposed elements exhibited satisfactory performance and always converged to the exact solutions. To solve a sheet-metal member with higher efficiency and flexibility, Franciosa et al. [15] defined a novel triangular shell element. Proficiency was obtained by combining the hybrid quadrilateral and triangular elements. They found that new hybrid elements predict the performance of shell elements better than those of conventional displacement-based elements. In 2011, Duan et al. [16] analyzed the cracking patterns in plate bending problems by using new triangular elements. The obtained outcomes demonstrated that their new schemes had very good agreement with the analytical solutions, even with big mesh sizes. These investigators reported that their elements exhibited high accuracy and efficiency. In another research, Mu and Zhang [17] utilized six node triangular elements to assess the cracking in plate members. They have tested their elements with several benchmarks by focusing on different mesh sizes. The mesh dependencies illustrated the efficiency and toughness of the planned new elements. In 2016, Zhuang et al. [18] evaluated the behavior of thick plates by considering the influence of shear stress over the thickness using new triangular elements. Their proposed elements had six and nine degrees of freedom. After presenting the formulation, they evaluated their method to anticipate the performance of thin plates. Several numerical benchmarks illustrated the efficiency and precision of their elements. Ma and Chen [19] developed a new triangular stress-based element with eighteen degrees of freedom. In addition, a refined expected stress element scheme was established to enhance the accuracy of their element. The obtained outcomes showed that this element certainly had higher accuracy and could pass the improved patch test compared to those of the displacement-based elements.

In 2010, Zhao et al. [20] employed energy techniques to develop an eighteen-degrees-of-freedom triangular element. In this evaluation, a feeble continuousness state of the axisymmetric uncharacteristic element model was presented using the couple stress scheme. Numerical consequences demonstrated that their recommended element could be utilized for analyzing the size effect and had appropriate convergence efficiency. Kaveh and Daei [21] used an optimization technique to increase the accuracy of triangular elements. For this aim, different examples were solved and showed the efficiency of their proposed algorithm. Hu et al. [22] defined a new element using mesh-free-enriched triangular elements for analyzing 2D large deformation problems. Their numerical results exhibited the high correctness and efficiency of the suggested displacement-based element. To formulate a rank adequate for the six-node elements, a minimum of six wave modes from three basis sites is compulsory [23]. These investigators found that the near-exact results could be obtained by using wavelet techniques. Huang et al. [24] considered drilling rotation degrees to formulate a triangular element. They declared that the drilling factor of their element could properly carry over the twisting moment, relative to those elements proposed previously. To advance the performance of triangular and rectangular plate bending elements, Kaveh and Koohestani [25] studied the graph-theoretical for the force scheme. They solved different problems using their elements and declared that the recommended elements had high accuracy in predicting the plate behavior.

In 2019, Chen and Li [26] proposed a 3D triangular element using a B-net system with fifteen nodes. They put the TPS15 element through its paces with various numerical cases, counting one that comprises the hexahedral element. The numerical consequences revealed that the spline elements have greater correctness in most circumstances, notably for deformed models, as compared to the Isoparametric elements. Cui et al. [27] were the ones who demarcated using triangular and quadrilateral elements for structure examination. Additionally, this approach is used to create high-order quadrilateral transition

components. With no need for the requirement to divide the components into lesser levelling cells, triangular and quadrilateral high-order CS-FEMs may be formed. They also discovered that in their formulation, the edge nodes of the high-order elements may be arbitrarily positioned, which is not allowed in a typical high-order FEM system. In another evaluation, Zander et al. [28] proposed anisotropic multi-level quadrilateral and triangular elements. The given findings establish the suggested technique as an automated, anisotropic multi-level process for quadrilateral and triangular meshes, with minimal implementation complexity and no limits imposed by subjective hanging nodes and the accompanying dead-lock difficulties. Kamiski [29] used the stochastic perturbation-based FEM to perform ambiguity examination in solid procedures with unchanging and triangular elements. The structural reactions of numerous automatic schemes are investigated utilizing their fundamental probabilistic properties, which have been confirmed using a probabilistic semi-analytical technique. Recently, Cho [30] used the FEM approach to do a non-linear bending analysis of a plate lying on an elastic basis. These non-dimensional characteristics are investigated in terms of foundation stiffness, gradient pattern, plate feature and width-thickness fractions, and boundary state. The parametric tests reveal that such factors have a large impact on both non-dimensional quantities.

As it is reported in the literature, using the stress function plays an influential function in improving the elemental response accuracies. Two elements were formulated using the conventional finite element technique, with the imposition of compatibility conditions. Moreover, two other elements were established based on the stress functions. Therefore, two of them are displacement-based compatible triangular elements, which are named Karimi Pour Compatible Triangular (KCT) and Noroozinejad Compatible Triangular (NCT) elements. Besides, two other stress-based incompatible triangular elements are also suggested with the names of Karimi Pour Incompatible Triangular (KIT) KIT and Noroozinejad Incompatible Triangular (NIT) elements. Compatible elements are those that satisfy the displacement compatibility requirement. This means that the displacement at all points is not a function of the path, and there exists a uniquely defined displacement field. Conversely, incompatible elements violate the displacement compatibility requirement. Incompatible elements were introduced to correct the strains produced by incompatible displacements, achieving excellent results for elements and for this aim, formulations have been established based on stress functions. Therefore, compatible elements provide the displacement responses with higher accuracy, but incompatible elements provide the stress responses with higher accuracy. This is the first time that, using the stress function, we can develop elements predicting both stress and displacement responses with higher accuracy. Based on this fact, four new triangular elements, compatible and incompatible, are developed for analyzing the plate bending structures. They are named KIT, NIT, KCT, and NCT. It should be noted that the differences between the proposed elements come from their degrees-of-freedom arrangements. To show the competence of the projected elements, several problems are solved with the recommended four elements. Numerical results illustrate that good outcomes for the displacements, and specifically for the stresses, could be achieved by using these elements. Moreover, using stress functions to formulate the elements reduces the processing time of analyses.

2. Plate Bending Governing Equations

The deformed shape of a plate could be determined by the displacement function at different points of the plate. Generally, the following equation could be utilized to determine the plate deformation, as demonstrated in Fig. 1.
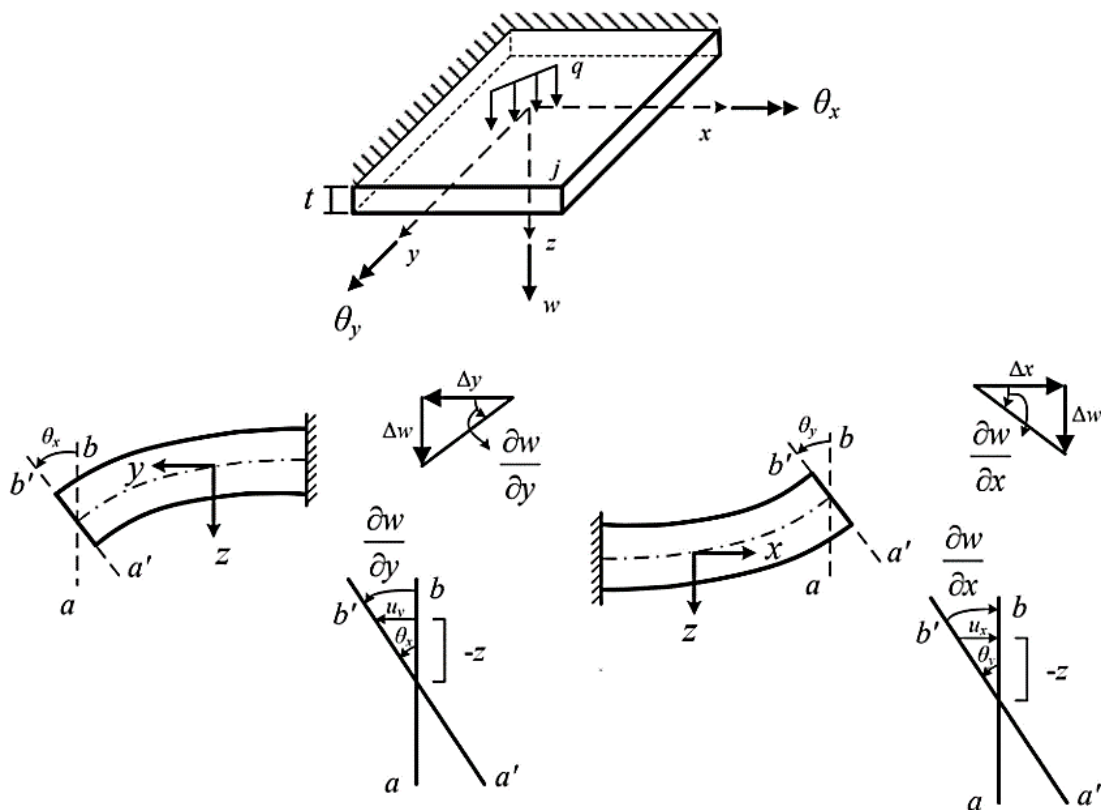
Fig. 1. Displacement and rotations of an infinitesimal plate bending

$$\{\theta\} = \begin{Bmatrix} \theta_x \\ \theta_y \end{Bmatrix} = \begin{bmatrix} \dfrac{\partial}{\partial y} \\ -\dfrac{\partial}{\partial x} \end{bmatrix} w \ , \tag{1}$$

$$\{u\} = \begin{Bmatrix} u_x \\ u_y \\ u_z \end{Bmatrix} = \begin{Bmatrix} z\theta_y \\ -z\theta_x \\ w \end{Bmatrix} , \tag{2}$$

in which, $\{\theta\}$ and $\{u\}$ indicate the rotational and transitional deformations. According to the Kirchhoff hypothesis, the plate rotations are related to the derivatives of the displacement function. Besides, the non-zero strains could be defined by considering the corresponding curvatures, as follows:

$$\{\varepsilon\} = \begin{Bmatrix} \varepsilon_x \\ \varepsilon_y \\ \varepsilon_{xy} \end{Bmatrix} = \begin{bmatrix} \dfrac{\partial}{\partial x} & 0 \\ 0 & \dfrac{\partial}{\partial y} \\ \dfrac{\partial}{\partial y} & \dfrac{\partial}{\partial x} \end{bmatrix} \begin{Bmatrix} u_x \\ u_y \end{Bmatrix} = -z \begin{bmatrix} \dfrac{\partial^2}{\partial x^2} \\ \dfrac{\partial^2}{\partial y^2} \\ 2\dfrac{\partial^2}{\partial x \partial y} \end{bmatrix} w \ . \tag{3}$$

In the transverse directions, both normal (ε_{zz}) and shear (ε_{xz} and ε_{yz}) strains are zero. The integral through the plate thickness is used to outline the moments at a given position. To satisfy the equilibrium conditions, the moments, $\{M\}$, and shear forces, $\{V\}$, are corresponding to the integrals of out-of-plane shear stresses according to the following formulas:

$$\{M\} = \begin{Bmatrix} M_x \\ M_y \\ M_{xy} \end{Bmatrix} = \int_{-t/2}^{t/2} z \begin{Bmatrix} \sigma_x \\ \sigma_y \\ \tau_{xy} \end{Bmatrix} dz \ , \tag{4}$$

4

$$\{V\} = \begin{Bmatrix} V_x \\ V_y \end{Bmatrix} = \int_{-t/2}^{t/2} \begin{Bmatrix} \tau_{xz} \\ \tau_{yz} \end{Bmatrix} dz . \tag{5}$$

By considering the applied transverse load, q, the following equilibrium equations should be satisfied:

$$\frac{\partial V_x}{\partial x} + \frac{\partial V_y}{\partial y} + q = 0 , \tag{6}$$

$$\frac{\partial M_x}{\partial x} + \frac{\partial M_{yx}}{\partial y} - V_x = 0 , \tag{7}$$

$$\frac{\partial M_y}{\partial x} + \frac{\partial M_{xy}}{\partial y} - V_y = 0 . \tag{8}$$

After eliminating the shear forces, V_x and V_y , from the last relations, the following governing equation is derived:

$$\frac{\partial^2 M_x}{\partial x^2} + \frac{\partial^2 M_y}{\partial y^2} + 2\frac{\partial^2 M_{xy}}{\partial x \partial y} + q = 0 . \tag{9}$$

The moments and strains are related as follows:

$$[D_m] = \frac{Et^3}{12(1-v^2)} \begin{bmatrix} 1 & v & 0 \\ v & 0 & 0 \\ 0 & 0 & \frac{1-v}{2} \end{bmatrix} , \tag{10}$$

$$\{M\} = [D_m]\{\varepsilon\} . \tag{11}$$

3. Formulating KCT and NCT elements

In this study, four triangular elements with thirteen nodes are developed. All elements are exposed in Fig. 2. These new plate-bending elements are presented based on the demonstrated degrees of freedom. Two of them are compatible, and the other ones are incompatible triangular elements. It should be noted that all four proposed elements are based on the full 5th-degree function with 21 terms, as follows:

$$\begin{aligned}
w(\xi_i, \xi_j, \xi_k) = {} & \alpha_1\xi_i^5 + \alpha_2\xi_i^4\xi_j + \alpha_3\xi_i^4\xi_k + \alpha_4\xi_i^3\xi_j^2 + \alpha_5\xi_i^3\xi_j\xi_k + \alpha_6\xi_i^3\xi_k^2 \\
& + \alpha_7\xi_i^2\xi_j^3 + \alpha_8\xi_i^2\xi_j^2\xi_k + \alpha_9\xi_i^2\xi_k^2\xi_j + \alpha_{10}\xi_j^2\xi_k^3 + \alpha_{11}\xi_j^4\xi_i \\
& + \alpha_{12}\xi_i\xi_j^3\xi_k + \alpha_{13}\xi_i\xi_j^2\xi_k^2 + \alpha_{14}\xi_i\xi_j\xi_k^3 + \alpha_{15}\xi_i\xi_k^4 + \alpha_{16}\xi_j^5 \\
& + \alpha_{17}\xi_j^4\xi_k + \alpha_{18}\xi_j^3\xi_k^2 + \alpha_{19}\xi_j^2\xi_k^3 + \alpha_{20}\xi_j\xi_k^4 + \alpha_{21}\xi_k^5
\end{aligned} \tag{12}$$

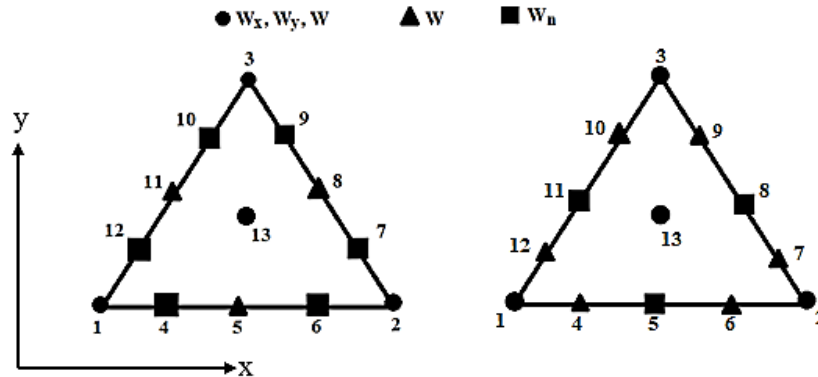Fig. 2. Projected triangular elements: (a) KCT and KIT, (b) NCT and NIT

Where ξ_i, ξ_j and ξ_k are Lagrangian normalized finite element coordinates which were discussed in previous studies in detail [31]. According to the Fig. 2, the element nodal displacement for KCT, $\{d\}_{KCT}$, has the subsequent arrangement:

$$\{d\}_{KCT} = \{ w_{x1} \ w_{y1} \ w_1 \ w_{x2} \ w_{y2} \ w_2 \ w_{x3} \ w_{y3} \ w_3 \ w_{n4} \ w_5 \ w_{n6}$$
$$w_{n7} \ w_8 \ w_{n9} \ w_{n10} \ w_{11} \ w_{12} \ w_{x13} \ w_{y13} \ w_{13}\} . \tag{13}$$

In addition, NCT has the following elements nodal displacement, $\{d\}_{NCT}$:

$$\{d\}_{NCT} = \{ w_{x1} \ w_{y1} \ w_1 \ w_{x2} \ w_{y2} \ w_2 \ w_{x3} \ w_{y3} \ w_3 \ w_4 \ w_{n5} \ w_6$$
$$w_7 \ w_{n8} \ w_9 \ w_{10} \ w_{n11} \ w_{12} \ w_{x13} \ w_{y13} \ w_{13} \} . \tag{14}$$

The next equation is established to determine the polynomial matrix, $[P]$:

$$w(\xi_i, \xi_j, \xi_k) = [P]\{\alpha\} , \tag{15}$$

where, $\{\alpha\}$ is the unknown parameter. To find the interpolation matrix, $[N]$, the inverse geometric matrix, $[G]^{-1}$, is utilized as follows:

$$[N] = [P][G]^{-1} . \tag{16}$$

Having interpolation functions, the strain matrix, $[B]$, and elemental stiffness, $[K]$, can be calculated by the next relations:

$$\{\varepsilon\} = [B]\{d\} , \tag{17}$$

$$[B] = \left\{ \begin{matrix} -\dfrac{\partial^2}{\partial x^2} \\ -\dfrac{\partial^2}{\partial y^2} \\ -2\dfrac{\partial^2}{\partial x \partial y} \end{matrix} \right\} [N] , \tag{18}$$

$$[K] = \int_0^1 \int_0^1 [B]^T [D_m][B]|j|d\xi_i d\xi_j . \tag{19}$$

It should be mentioned that both compatible elements, KCT and NCT, satisfied another condition. To establish these elements, the following compatibility equation is imposed on the strains:

$$\frac{\partial^2 \varepsilon_x}{\partial x^2} + \frac{\partial^2 \varepsilon_y}{\partial y^2} - 2\frac{\partial^2 \varepsilon_{xy}}{\partial x \partial y} = 0 . \tag{20}$$

4. Formulating KIT and NIT elements

By taking advantage of the stress functions, two new incompatible elements, named KIT and NIT, are proposed. The element complementary energy functional (Π_C^*) is represented in the following arrangement:

$$\Pi_C^* = U_C^* + V_C^* = \frac{1}{2}\int \int_{A^e} \{\sigma\}^T [C]\{\sigma\} t dA - \int_\Gamma \{T\}^T [u] t ds , \tag{21}$$

$$U_C^* = \frac{1}{2}\int \int_{A^e} \{\sigma\}^T [C]\{\sigma\} t dA , \tag{22}$$

$$V_C^* = -\int_\Gamma \{T\}^T [u] t ds , \tag{23}$$

$$[C] = \frac{(1-v^2)}{E} \begin{bmatrix} 1 & -\dfrac{v}{1-v} & 0 \\ -\dfrac{v}{1-v} & 1 & 0 \\ 0 & 0 & 2(1+\dfrac{v}{1-v}) \end{bmatrix} . \tag{24}$$

The matching energy inside the element and sides of the element borders, correspondingly, are U_C^* and V_C^*. Furthermore, the elements' thickness, stress vector, surface traction force across element borders, and displacement vector lengthwise element boundaries, as well as the elastic plasticity matrix, are indicated by t, $\{\sigma\}$, $\{T\}$, $[u]$, and $[C]$. In these relations, E and v are elastic moduli and Poisson's ratio, correspondingly. The stress vector $\{\sigma\}$ may be represented as below using the stress function, φ:

$$\{\sigma\} = \begin{Bmatrix} \sigma_x \\ \sigma_y \\ \tau_{xy} \end{Bmatrix} = \begin{Bmatrix} \frac{\partial^2 \varphi}{\partial y^2} \\ \frac{\partial^2 \varphi}{\partial x^2} \\ -\frac{\partial^2 \varphi}{\partial x \partial y} \end{Bmatrix} = \{\tilde{R}(\varphi)\}, \tag{25}$$

$$[L] = \begin{bmatrix} l & 0 & m \\ 0 & m & l \end{bmatrix}. \tag{26}$$

The route cosines of the outside normal of each element border, l and m, are stated in the next forms:

$$l = \frac{dy}{ds}, \quad m = -\frac{dx}{ds}. \tag{27}$$

Utilizing the stress function vector, $\{\tilde{R}(\varphi)\}$, the complementary energy can be presented as:

$$U_C^* = \frac{1}{2} \int \int_{A^e} \{\tilde{R}(\varphi)\}^T [C] \{\tilde{R}(\varphi)\} dA, \tag{28}$$

$$V_C^* = -\int_\Gamma [[L]\{\tilde{R}(\varphi)\}]^T t\, ds, \tag{29}$$

$$\Pi_C^* = U_C^* + V_C^* = \frac{1}{2} \int \int_{A^e} \{\tilde{R}(\varphi)\}^T [C] \{\tilde{R}(\varphi)\} dA - \int_\Gamma [[L]\{\tilde{R}(\varphi)\}]^T t\, ds. \tag{30}$$

The elemental complementary energy covering the stress function is a valuable instrument for applying to the finite element technique. For the plate problems deprived of body forces, the stress purpose could be defined by the following formula:

$$\nabla^4 \varphi = \frac{\partial^4 \varphi}{\partial y^4} + 2 \frac{\partial^4 \varphi}{\partial x^2 \partial y^2} + \frac{\partial^4 \varphi}{\partial x^4}. \tag{31}$$

The methods below should be followed to find acceptable trial stress functions for creating an innovative element:

1 – the elementary analytical answers of the stress purpose, which contain terms from the last order to the advanced order, should be chosen [32];

2 – in Cartesian Coordinates, the resultant stress areas should be full.

There are different analytical solutions for stress function for the defined degrees of freedom. In this article, the stress function is established in terms of unknown parameters, and in the general following form [33]:

$$\varphi = \sum_{i=1}^n \varphi_i \beta_i. \tag{32}$$

The number of analytical responses for the stress purpose is φ_i (i=1-n), while the number of unknown constants is β_i (i=1-n). It should be noted that the number of degrees of freedom is one unit fewer than the value of n. The stress function may be calculated as per the number of nodes and degrees of freedom in the element. The analytical answers for stress function and stresses associated with KIT and NIT elements are found using the supplied equations. All stress function constraints are gathered and displayed in Tables 1 and 2 after searching, assessing, and corresponding. To consider φ_i term in tables 1 and 2, generally, the authors assumed a total of 21 terms. The first term was number one (1) ($\varphi_1 = 1$) and because the derivatives of number (1) are zero, this term is practically ineffective and is not presented and considered in the table. While, in general, 21 semesters are considered: the number (1) + 20 terms presented in Table 1 ($\varphi_1, \varphi_2, \ldots \varphi_{20}$), for example. The same process was followed and recommended by Fu et al [33] for 2D analysis elements, as the basic benchmark and study.

Table 1. Analytical solutions for the KIT's stress function and stressors

	i	1	2	3	4	5	6	7	8	9	10	11
KIT	φ_i	x^2	xy	y^2	x^3	x^2y	y^2x	y^3	x^4	x^3y	y^3x	y^4
	σ_x	0	0	2	0	0	2x	6y	0	0	6xy	$12x^2$
	σ_y	2	0	0	6x	2y	0	0	$12y^2$	6xy	0	0
	τ_{xy}	0	-1	0	0	-2x	-2y	0	0	$-3x^2$	$-3y^2$	0
	i	12	13	14	15	16	17	18	19		20	
	φ_i	y^3x	y^2x^2	x^5	x^5	y^4x	x^5	x^4y	$x^4y-y^3x^2$		$x^3y^2-y^3x^2$	
	σ_x	6xy	$2x^2$	0	0	$12y^2x$	$20y^3$	0	$-6yx^2$		$2x^3-6yx^2$	
	σ_y	0	$2y^2$	$20x^3$	$20x^3$	0	0	$12x^2y$	$12x^2y-2y^3$		$6xy^2-2y^3$	
	τ_{xy}	$-3y^2$	-4xy	0	0	$-4y^3$	0	$-4x^3$	$-4x^2+6y^2x$		$-6x^2y+6y^2x$	

Table 2. Analytical solutions for the NIT's stress function and stressors

	i	1	2	3	4	5	6	7	8	9	10	11
NIT	φ_i	x	y	x^2	xy	y^2	$-x^2-y^2$	x^3	$-x^2y-xy^2$	y^3	x^4	x^2y^2
	σ_x	0	0	0	0	2	-2	0	$-2x$	6y	0	$2x^2$
	σ_y	0	0	2	0	0	-2	6x	$-2y$	0	$12x^2$	$2y^2$
	τ_{xy}	0	0	0	1	0	$2x+2y$	0	$2x+2y$	0	0	$-4xy$
	i	12	13	14	15	16	17	18	19		20	
	φ_i	$-x^3y-xy^3$	x^4	x^5	x^4y	xy^4	y^5	$-x^3y^2-x^2y^3$	x^6		x^5y	
	σ_x	$-6xy$	0	0	0	$12xy^2$	$20y^3$	$-2yx^3$	0		0	
	σ_y	$-6xy$	$12x^2$	$20x^3$	$12x^2y$	0	0	$-6xy^2-2y^3$	$30x^4$		$20x^3y$	
	τ_{xy}	$3x^2+3y^2$	0	0	$-4x^3$	$-4x^3$	0	$6x^2y+6xy^2$	0		$5x^4$	

Upon substitution of Eq. (32) into Eqs. (28) and (29), the succeeding relations could be found:

$$U_C^* = \frac{1}{2}\{\beta\}^T[F]\{\beta\}, \tag{33}$$

$$V_C^* = -\{\beta\}[F]\{\beta\}^T, \tag{34}$$

$$[F] = \int\int_{A^e}[S]^T[C][S]t\,dA. \tag{35}$$

The stress vector forms the matrix [S]. Matrix [F] is found in Eq. (35). After performing the required calculations, the subsequent outcome for the incompatible element, KIT, is achieved:

$$[S]_{KIT} = \begin{bmatrix} 0 & 0 & 2 & 0 & 0 & 2x & 6y & 0 & 0 & 6xy & 12x^2 & 6xy \\ 2 & 0 & 0 & 6x & 2y & 0 & 0 & 12y^2 & 6xy & 0 & 0 & 0 \\ 0 & -1 & 0 & 0 & -2x & -2y & 0 & 0 & -3x^2 & -3y^2 & 0 & -3y^2 \end{bmatrix}$$
$$\begin{bmatrix} 2x^2 & 0 & 0 & 12y^2x & 20y^3 & 0 & -6yx^2 & 2x^3-6yx^2 \\ 2y^2 & 20x^3 & 20x^3 & 0 & 0 & 12x^2y & 12x^2y-2y^3 & 6xy^2-2y^3 \\ -4xy & 0 & 0 & -4y^3 & 0 & -4x^3 & -4x^2+6y^2x & -6x^2y+6y^2x \end{bmatrix} \tag{36}$$

For another element, NIT, the subsequent result is reached:

$$[S]_{NIT} = \begin{bmatrix} 0 & 0 & 0 & 0 & 2 & -2 & 0 & -2x & 6y & 0 & 2x^2 & -6xy \\ 0 & 0 & 2 & 0 & 0 & -2 & 6x & -2y & 0 & 12x^2 & 2y^2 & -6xy \\ 0 & 0 & 0 & 1 & 0 & 2x+2y & 0 & 2x+2y & 0 & 0 & -4xy & 3x^2+3y^2 \end{bmatrix} \tag{37}$$

$$\begin{bmatrix} 0 & 0 & 0 & 12xy^2 & 20y^3 & -2yx^3 & 0 & 0 \\ 12x^2 & 20x^3 & 12x^2y & 0 & 0 & -6xy^2-2y^3 & 30x^4 & 20x^3y \\ 0 & 0 & -4x^3 & -4x^3 & 0 & 6x^2y+6xy^2 & 0 & 5x^4 \end{bmatrix}$$

By defining the matrix [H], the elemental complementary energy containing the nodal displacements can be formed:

$$[H] = \int_{\Gamma_{ij}} [S]^T [L]^T [N] tds + \int_{\Gamma_{jk}} [S]^T [L]^T [N] tds + \int_{\Gamma_{kl}} [S]^T [L]^T [N] tds . \tag{38}$$

Here, Γ_{ij}, Γ_{jk} and Γ_{kl} denote the element edges. By inserting Eq (33) and (34) into Eq (30), the succeeding element complementary energy purpose is originated:

$$V_C^* = -\{\beta\}^T [H]\{d\} , \tag{39}$$

$$\Pi_C^* = \frac{1}{2}\{\beta\}^T [F]\{\beta\} - \{\beta\}^T [H]\{d\}. \tag{40}$$

To calculate the elemental answer, by utilizing the value of the lowermost matching energy, Π_C^* must be diminished:

$$\frac{\partial \Pi_C^*}{\partial \beta} = 0. \tag{41}$$

After scheming the nodal displacement, $\{d\}$, the unidentified constant, $\{\beta\}$, can be attained by the subsequent formula:

$$\{\beta\} = [F]^{-1}[H]\{d\}. \tag{42}$$

Substitution of Eq. (42) into Equation (40) yields:

$$\Pi_C^* = \frac{1}{2}\{d\}^T [K^*]\{d\}, \tag{43}$$

$$[K^*] = \big[[F]^{-1}[H]\big]^T [H], \tag{44}$$

in which, matrix $[K^*]$ could be measured as the corresponding stiffness matrix. This matrix is utilized in a common finite element analysis. After the discovery of the element nodal displacements, the element stresses could be printed as:

$$\{\sigma\} = [S][F]^{-1}[H]\{d\}. \tag{45}$$

Having the stress function for each element, the stresses for all structural points will be in hand.

5. Numerical Tests

In this part, the presentation of the recommended elements is shown by analyzing eleven well-known benchmark problems. The following subsections will describe all the specifications of the plate-bending structures. Moreover, proper discussions will be provided about the abilities of the new formulations.

5.1. Example #1

As illustrated in Fig. 3, a simply supported plate is considered and evaluated. The modulus of elasticity, Poisson's ratio, and the thickness of the plate are 1.00, 0.30, and 0.05, correspondingly. This structure is exposed to a load established based on Hybrid Equilibrium Elements for Kirchhoff plates [31]. On the plate, three loadings are well-thought-out: a uniform distributed load (UDL), two-unit line loads laterally the axis of symmetry, and a unit point load in the center, all designated in a steady arrangement of units. Line loads of two units are equivalent to 0.5 units of force each unit length. A point load is 0.25 units of force per unit length. After utilizing the proposed elements, the obtained consequences are represented in Tables 3 and 4 for different meshes.
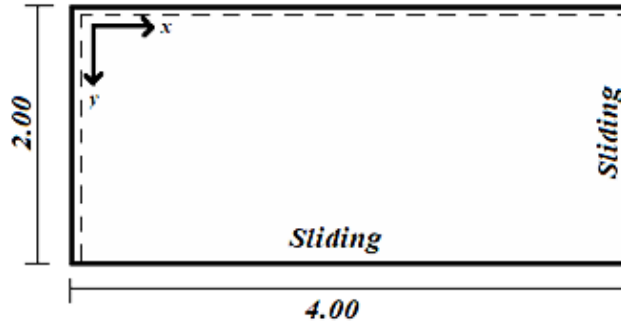
Fig. 3. Simply supported rectangular plate

To compare the elemental abilities, the analysis time is also evaluated, which shows the speed of solutions. The twisting moment at the junction of the two upright descending supports is zero in this example. As a result, the basic requirement is kinematic, and any suitable solution is highly sensitive to it. Based on this fact, the achieved results reveal that two new compatible displacement-based proposed elements (NCT and KCT) have the apt act. Furthermore, all answers prove that supplementary precise answers could be reached by using stress-based functions. NIT provides near-exact solutions for both displacements and stresses, while the other two components provide precise answers, comparative to those of compatible displacement-based elements, KCT and NCT. It is worth mentioning that the analysis time has considerably declined as a result of using stress-based suggested elements.

Table 3. Computed displacement at the plate center

	KCT	NCT	KIT	NIT	EXACT
UDL	1.42853E+04	1.42954E+04	1.42882E+04	1.42960E+04	1.42962E+04
Line	1.83716E+04	1.84857E+04	1.84016E+04	1.84888E+04	1.84892E+04
point	5.77254E+03	5.77824E+04	5.77542E+03	5.77909E+04	5.77915E+04
Average Time (Sec)	21	16.9	12.4	8.6	-

Table 4. Stress and displacement products at the center

Element	Mesh	Displacement	Stress	Time (Sec)
KCT	8×8	1.20712	1.81701	6.8447
	12×12	1.21539	1.83670	7.4197
	16×16	1.21726	1.84353	8.3972
	32×32	1.22382	1.85016	9.7197
KIT	8×8	1.21134	1.82812	7.3967
	12×12	1.21399	1.83982	8.6157
	16×16	1.21758	1.84626	9.6047
	32×32	1.22054	1.85620	10.697
NCT	8×8	1.22803	1.85328	5.0737
	12×12	1.23536	1.85718	5.6947
	16×16	1.23723	1.86459	6.8562
	32×32	1.23910	1.86946	7.5577
NIT	8×8	1.22956	1.85992	5.0000
	12×12	1.23645	1.86142	5.5986
	16×16	1.23864	1.86558	6.3548
	32×32	1.23938	1.86976	6.9875
Exact		1.23942	1.86985	-

5.2. Example #2

In this benchmark, a double symmetry rectangular plate in Fig. 4 is considered. The answer for this structure, which agrees with one of the relations of the Levy-type answer [31]. The elastic moduli, Poisson's ratio, and the thickness of the plate are assumed to be 1.00, 0.30, and 0.05, respectively. As reported, the precise value of the normal rotations corresponding to the exact displacements is ∓ 610.957276165364 $sin(5.49778714378214x)$, according to Ref. [32]. At the simply supported sides with unchanging y, it is described that if this example is scrutinized with equilibrium elements, the consistent answers are not severely balanced. As the polynomial moment is unable precisely to epitomize the sinusoidal load. However, it is likely to get nearby balanced answers by seeing the delinquent with levied displacements. For the suggested formulations, the achieved responses for the diverse elements are represented in Table 5. Regarding the computed responses, the new stress-based elements KIT and NIT have more truthful stress and displacement answers, compared to those of compatible displacement-based elements (KCT and NCT). Achieved responses after solving this problem demonstrate that both presented stress-based elements play an important role in reducing the analyzing time.
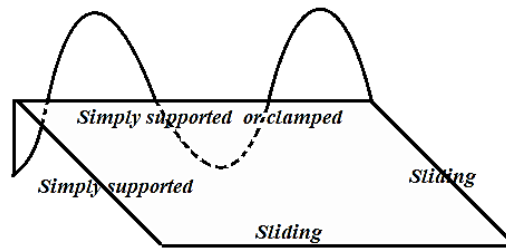

Fig. 4. With a sinusoidal action, a double symmetry simplification of the rectangular plate is achieved

Table 5. Moments computed in the double symmetry plate's center

		m_{xx}	m_{yy}	m_{xy}	Time
UDL	KCT	2.27574E-01	4.25147E-01	1.04587E-03	9.94
	NCT	2.31478E-01	4.92548E-01	2.14587E-02	9.72
Line	KCT	2.645874E-01	5.75645E-01	2.87489E-02	8.45
	NCT	2.96654E-01	6.02577E-01	3.84156E-02	8.19
Point	KCT	1.28258E-01	1.92547E-01	-1.00081E-02	7.85
	NCT	1.37895E-01	2.12587E-01	1.43289E-02	7.50
UDL	KIT	2.29574E-01	4.49147E-01	1.83278E-03	8.42
	NIT	2.32178E-01	4.93548E-01	2.15002E-02	8.15
Line	KIT	2.75162E-01	5.96681E-01	3.18754E-02	7.98
	NIT	2.96892E-01	6.13578E-01	3.85119E-02	6.82
Point	KIT	1.32324E-01	1.99857E-01	1.22854E-02	5.65
	NIT	1.39588E-01	2.13354E-01	1.44295E-02	5.02
UDL	Exact	2.32280E-01	4.93748E-01	2.15210E-02	-
Line		2.96987E-01	6.15874E-01	3.85248E-02	
Point		1.40581E-01	2.13587E-01	1.44358E-02	

5.3. Example #3

In this subsection, another rhombic and symmetric plate bending is analyzed. All sides of this structure have a unit length. There are two free and two simply supported edges in this plate. This structure is proved in Fig. 5 [31]. The performance of this plate is studied under a uniformly distributed load. It should be noted that because of the regularity of the plate, only one-half of the structure is evaluated by considering sliding support on the symmetry line. Furthermore, the elastic moduli (E) and Poisson's ratio

(v) of the plate were 1.0 and 0.3, correspondingly. Here, both displacement and stress mechanisms along the diagonals of the plate are measured. The obtained consequences are signified in Table 6. These responses are also compared with each other. According to the obtained outcomes, the stress-based elements, KIT and NIT, give very good outcomes against the suggested compatible displacement-based elements. When utilizing the NIT element, the solution time is significantly dropped. This is a good merit of the suggested element, which reduces the computational time required for solving complex problems.
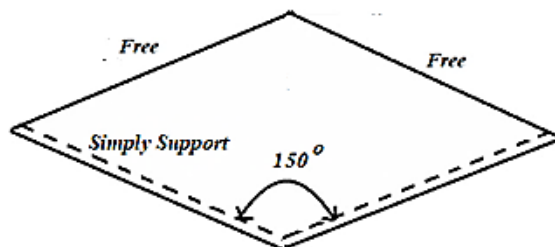

Fig. 5. Rhombic and symmetric plate bending

Table 6. Stress and displacement conclusions of rhombic and symmetric plate bending

Element	Displacement	Stress	Time
KCT	1.506829	2.462964	8.0017
KIT	1.512062	2.497962	8.5537
NCT	1.522757	2.501928	6.2307
NIT	1.533489	2.518971	3.5487
Exact	1.536881	2.524298	-

5.4. Example #4

In this portion, one quadrant of a circular plate is evaluated with diverse meshes, as illustrated in Fig. 6. All obtained outcomes along with the measured analysis time, are listed in Table 7. Moreover, the responses of the simply supported border circumstances are figured for a thick (R/t = 5/l) and a moderately thin (R/t = 5/0. l) plate [35]. The material characteristics are E = 10.92, v = 0.3. The uniform load q is 1.0. It is observed from Table 7 that the presented elements own high correctness. Once more, the responses illustrate that the new elements are accomplished of trappings the meticulous answers for the plate bending problems. In addition, less time is needed when the NIT element is utilized.
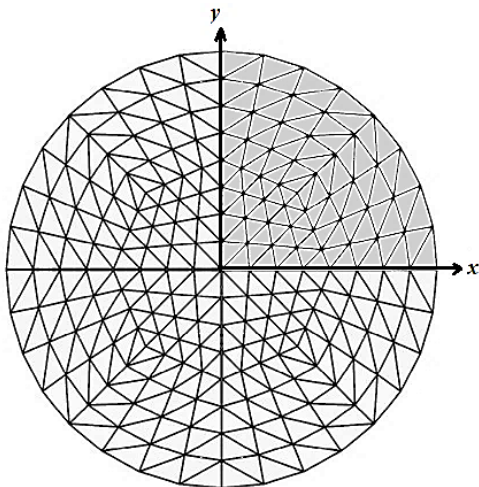

Fig. 6. Characteristic mesh for the quadrant of a circular plate

Table 7. Deformation and stress outcomes for the quadrant of a circular plate

Element	Mesh	$w\ (\times 10^2 ql^4/D)$	$M_y (\times 10 ql^2)$	Time
KCT	8×8	0.7840	0.9422	4.80
	12×12	0.7875	0.9479	5.30
	16×16	0.7888	0.9526	6.15
	32×32	0.7905	0.9548	7.30
KIT	8×8	0.7860	0.9489	5.28
	12×12	0.7892	0.9502	6.34
	16×16	0.7918	0.9542	7.20
	32×32	0.7926	0.9568	8.15
NCT	8×8	0.7872	0.9504	3.26
	12×12	0.7919	0.9524	3.80
	16×16	0.7931	0.9562	4.81
	32×32	0.7943	0.9587	5.42
NIT	8×8	0.7901	0.9518	1.14
	12×12	0.7926	0.9545	2.85
	16×16	0.7940	0.9572	3.54
	32×32	0.7944	0.9589	4.12
Exact		0.7945	0.9589	-

5.5. Example #5

In this portion, when the structure is under uniform loading, an angle plate that is simply supported on all ends is examined (q). Inner apex angles of 30" and 150" come from the skew angle. A typical mesh is illustrated in Fig. 7. The simply supported boundaries are preserved as easy, and the obtained answers are listed in Table 8 for the displacement at the plate center. It should be stated that the thickness of the plate is taken to be 1.0. The obtained results for a customary of meshes are associated with those of other elements and with the answer assumed in [35] for the 'thin' plate. For this example, the characteristics of the material are $E = 10 \times 10^6$, v = 0.3 and a = 100, respectively. Based on the accomplished answers, the formulations presented in this paper provide outstanding consequences at the slightest cost for all the suggested elements. According to Table 7, good performances are achieved by using new stress-based elements of KIT and NIT.
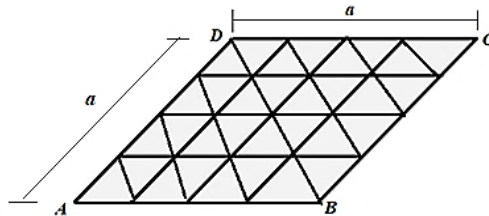

Fig. 7. A simply supported angle plate

Table 7. A simply supported skew plate

	Deflection at location					
	1	2	3	4	5	6
KCT	0.264	0.174	0.084	0.068	0.029	0.011
KIT	0.279	0.182	0.102	0.098	0.041	0.016
NCT	0.295	0.200	0.119	0.125	0.050	0.020
NIT	0.297	0.203	0.120	0.128	0.056	0.021
Exact	0.297	0.204	0.121	0.129	0.056	0.022

13

5.6. Example #6

Fig. 8 indicates a four-sided plate with a span-thickness fraction of a/t=50. The material characteristics of the plate are considered as E = 0.5 and the Poisson's ratio v=0.3. This structure is exposed to a regularly spread diagonal loading q. Since this plate has a symmetric shape, only a quarter of it is assessed in this subsection. Note that the edge consequence occurs in the regions close to the side AD. Accordingly, the dedicated element should be utilized for modeling the side sectors. Shang et al. [36] systematically investigated this target test by utilizing the semi-analytical segmentation technique. In this study, the obtained results by using different elements are provided for comparison purposes. All the answers are listed in Table 8. Numerical results indicate that NIT can reach the meticulous answers for this plate-twisting problem. As anticipated, by increasing the number of meshes, the accuracy of outcomes can be improved.
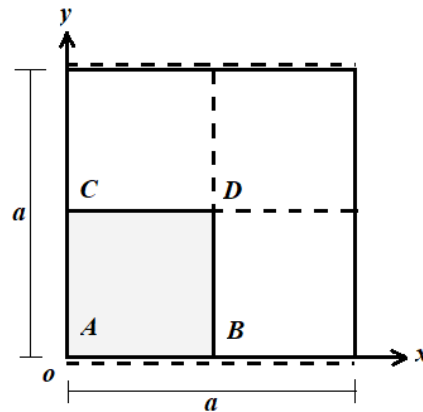

Fig. 8. Hardly supported square plate with two opposing edges

Table 8. Dimensionless deflections and stress

	Mesh N × N	16 × 16	32 × 32	100 × 100	Exact
$\dfrac{w_D}{qa^4}$	KCT	0.1088	0.1070	0.1068	0.1050
	KIT	0.1072	0.1062	0.1055	
	NCT	0.1060	0.1055	0.1051	
	NIT	0.1058	0.1053	0.1050	
$\dfrac{M_{xC}}{qa^2}$	KCT	0.0321	0.0301	0.0291	0.0268
	KIT	0.0290	0.0282	0.0278	
	NCT	0.0277	0.0273	0.0269	
	NIT	0.0275	0.0271	0.0268	
$\dfrac{M_{yC}}{qa^2}$	KCT	0.1289	0.1279	0.1268	0.1220
	KIT	0.1275	0.1268	0.1256	
	NCT	0.1259	0.1251	0.1240	
	NIT	0.1242	0.1237	0.1222	
$\dfrac{V_{yB}}{qa^2}$	KCT	0.1397	0.1369	0.1358	0.1300
	KIT	0.1380	0.1368	0.1336	
	NCT	0.1365	0.1350	0.1320	
	NIT	0.1338	0.1319	0.1308	

5.7. Example #7

A 60° rhombic plate is measured under a regularly dispersed oblique load (q) [36] (Fig. 9). The structural properties are, the thickness t = 0.1, span width a=5, and Poisson's ratio v = 0.3. It should be mentioned that the two boundaries, AB and DC, are simply supported, and the rest of them are free. All

structural elements are twisted because of the plate's rhombic figure, and it has four sides of the same length. Here, it is aimed to test the new formulations in the oblique meshes. After performing the analyses, the obtained numerical consequences are demonstrated in Table 9. Another time, it is detected that a respectable arrangement with the exact solutions is obtained by using the new proposed elements. Better answers for the displacement and also stress responses are taken when the incompatible stress-based elements, KIT and NIT, are used.
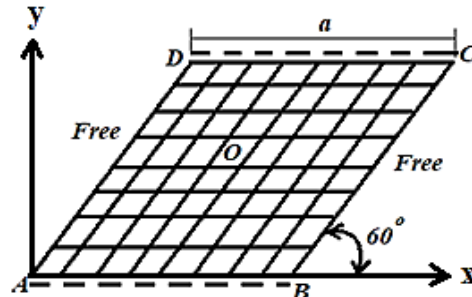

Fig. 9. The 60° skew plate with two contradictory boundaries

Table 9. Dimensionless deflections and stress result

	Mesh N × N	16 × 16	32 × 32	100 × 100	Exact
$\dfrac{w_o}{qa^4}$	KCT	0.0076	0.0068	0.0061	0.0041
	KIT	0.0058	0.0050	0.0045	
	NCT	0.0452	0.0447	0.0042	
	NIT	0.0449	0.0444	0.0040	
$\dfrac{M_{xC}}{qa^2}$	KCT	0.0524	0.0517	0.0508	0.0481
	KIT	0.0518	0.0509	0.0498	
	NCT	0.0496	0.0488	0.0482	
	NIT	0.0494	0.0487	0.0480	
$\dfrac{M_{yC}}{qa^2}$	KCT	0.0527	0.0519	0.0501	0.0482
	KIT	0.0508	0.0498	0.0490	
	NCT	0.0498	0.0490	0.0483	
	NIT	0.0496	0.0488	0.0481	
$\dfrac{V_{yB}}{qa}$	KCT	0.4251	0.4243	0.4232	0.4190
	KIT	0.4241	0. 4229	0.4219	
	NCT	0.4254	0.4231	0.4210	
	NIT	0.4227	0.4202	0.4189	

5.8. Example #8

As shown in Fig. 13, another 60° rhombic plate is exposed to a homogeneously dispersed oblique loading q, with the t = 0.1, a = 5, and v = 0.3 [36]. The plate boundaries, AB and DC, are simply supported, and the other two are both free or both soft and simply supported. Since elements are entirely skewed, since the plate's rhombic form, it could measure and validate the present formulations for the sloping meshes. The obtained outcomes are illustrated in Table 10. There, the stress-based elements, KIT and NIT, give very good results, relative to those found by the compatible displacement-based elements (KCT and NCT). According to the responses, it could be realized that the recommended elements have great correctness as a consequence of using the proper recommended purposes.
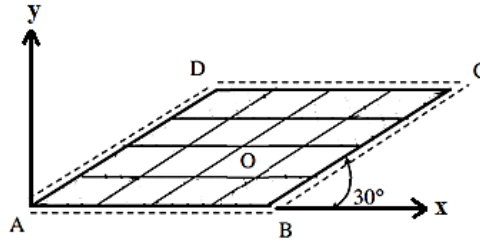
Fig. 10. Soft simply-supported plate

Table 10. Deflections and stress resultants for soft simply-supported plate

	Mesh	16×16	32×32	100×100	Exact
$\frac{w_O}{qa^4}$	KCT	0.0162	0.0156	0.0147	
	KIT	0.0151	0.0148	0.0145	0.0141
	NCT	0.0154	0.0150	0.0142	
	NIT	0.0148	0.0142	0.0140	
$\frac{M_{xC}}{qa^2}$	KCT	0.0624	0.0612	0.0587	
	KIT	0.0614	0.0601	0.0585	0.0581
	NCT	0.0613	0.0604	0.0582	
	NIT	0.0601	0.0586	0.0580	
$\frac{M_{yC}}{qa^2}$	KCT	0.0638	0.0621	0.0587	
	KIT	0.0611	0.0589	0.0585	0.0582
	NCT	0.0613	0.0602	0.0583	
	NIT	0.0598	0.0586	0.0581	
$\frac{V_{yB}}{qa}$	KCT	0.4367	0.4348	0.4321	
	KIT	0.4328	0.4302	0.4280	0.4290
	NCT	0.4351	0.4339	0.4310	
	NIT	0.4334	0.4321	0.4289	

5.9. Example #9

Fig. 11 expressions a quarter of a 4×4 sheet with a central circular opening of one radius. Lengthways $x_1 = 4$ and $x_2 = 4$, traction and double-traction, resulting from the succeeding axile equal displacement arena [37]:

$$\begin{Bmatrix} u_1 \\ u_2 \end{Bmatrix} = \frac{P}{2\mu r f_3}\left[f_1 - \frac{a}{1-2vf_2}\right]\begin{Bmatrix} \cos\theta \\ \sin\theta \end{Bmatrix} \tag{46}$$

$$f_1 = (v-1)a^4 + (2v-1)[2l^2 - r^2(v-1)]a^2 - 4(v-1)r^2l^2(2v-1)k_1\left(\frac{a}{l}\right) \tag{47}$$

$$f_2 = [a^2 - r^2(v-1)]K_0\left(\frac{a}{l}\right) - 2lr\,K_1\left(\frac{r}{l}\right) \tag{48}$$

$$f_3 = a^2 + 4l^2(v-1)K_1\left(\frac{a}{l}\right) + 2al\left(v - \frac{1}{2}\right)K_0\left(\frac{a}{l}\right) \tag{49}$$
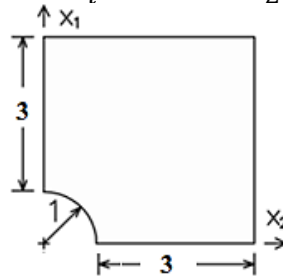

Fig. 11. A quarter of a square panel with a central circular cutout

Here, $a = 1$, ρ is the radial stress at $r = \infty$, K_n is the n-th directive adapted Bessel function of another type. The found consequences are demonstrated in Table 11 for different meshes. Numerical results illustrate that KIT and NIT can range the meticulous answers for the plate twisting with an opening region.

Table 11. Stress and displacement consequences of a square sheet with a dominant circular opening

Mesh	KCT	KIT	NCT	NIT
Normalized Stress				
4×4	1.21	1.18	1.11	1.09
8×8	1.19	1.15	1.05	1.03
16×16	1.17	1.12	1.01	1.00
Normalized displacement				
4×4	1.15	1.11	1.09	1.05
8×8	1.11	1.08	1.05	1.03
16×16	1.07	1.04	1.03	1.01

5.10. Example #10

In this test, an L-shaped plate is measured, which was solved by previous investigators [37]. This structure is measured as one-quarter of a double-symmetric edge, that is equally loaded on its perpendicular borders. At the Neumann frontier, a continuous load in the straight path $\bar{t}_1^P = -L^{-1}$kN/mm is performed (The load was performed as a thickness and dimension, as explained in Ref. [29]). For this plate, the maximum values of stress and displacement are evaluated, and represented in Table 12. As it is understood from the outcomes, the consequences of both displacement and stress can be predicted accurately by KIT and NIT. This fact demonstrates the efficiency of the offered stress functions. These obtained answers are also better than the compatible displacement-based elements' responses (KCT and NCT).
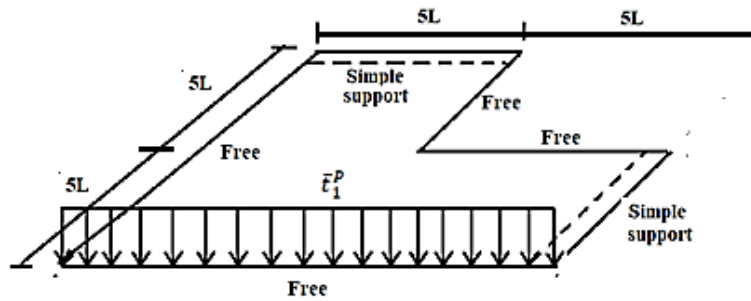

Fig. 12. Geometry of the center L-shaped domain plate

Table 12. Maximum value of stress and displacement for L-shaped plate

	Mesh	100×100	Time	Exact
Stress	KCT	0.012	2.845	
	KIT	0.010	1.846	0.010
	NCT	0.010	1.284	
	NIT	0.010	0.574	
Displacement	KCT	0.126	3.597	
	KIT	0.120	2.047	0.120
	NCT	0.120	2.005	
	NIT	0.120	0.975	

5.11.   Example #11

In this benchmark problem, an L-shaped plate is measured with a hole. This structure was also analyzed previously [37]. The sheet is a quarter of a double-symmetric edge with vertical bounds that are correspondingly loaded. As seen in Fig. 13, Dirichlet boundary circumstances related to equilibrium planes are enforced on the bottom border and right-hand side. The realized mathematical consequences are demonstrated in Table 13. According to the accomplished answers, the calculated stress components have high accuracy. It is also discovered that the NIT exhibits well acts. In fact, the proposed elements in this study could predict the stress components in different points of structures with low error. Lower analysis time is required if utilizing the NIT element.
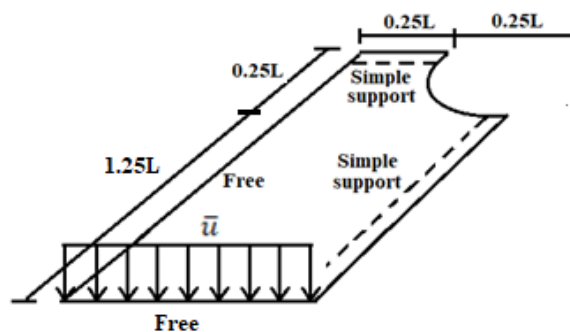

Fig. 13. Plate with a hole

Table 13. Stress and displacement products of the plate with a hole

Element	Displacement	Stress	Time
KCT	0.9388	1.23747	9.372
KIT	0.9405	1.23981	8.108
NCT	0.9531	1.24631	6.233
NIT	0.9532	1.24650	3.246
Exact	0.9534	1.24657	

6. Conclusion

Existing literature indicates that numerous research studies have demonstrated the limited suitability of displacement-based elements in accurately determining stress responses, despite their widespread popularity and applicability. This research aims to introduce four innovative elements designed for the assessment of plate-bending structures. Each of the recommended elements possesses thirteen degrees of freedom. Two elements were formulated using the conventional finite element technique, with the imposition of compatibility conditions. Moreover, two other elements were established based on the stress functions. Therefore, two of them are displacement-based compatible triangular elements, which are named Karimi Pour Compatible Triangular (KCT) and Noroozinejad Compatible Triangular (NCT) elements. Besides, other two stress-based incompatible triangular elements are also suggested with the names of Karimi Pour Incompatible Triangular (KIT) KIT and Noroozinejad Incompatible Triangular (NIT) elements. Compatible elements are those that satisfy the displacement compatibility requirement. This means that the displacement at all points is not a function of the path, and there exists a uniquely defined displacement field. Conversely, incompatible elements violate the displacement compatibility requirement. Incompatible elements were introduced to correct the strains produced by incompatible

18

displacements, achieving excellent results for elements and for this aim, formulations have been established based on stress functions. Therefore, based on stress functions, formulas for elements are developed. For the structural stresses, some fundamental analytical answers are assigned in this inquiry. The trial functions are aligned with each element by considering the degrees-of-freedom numbers. Unknown coefficients are ascertained by minimizing the complementary energy to achieve an accurate solution. A comparison is made between the outcomes obtained through these methods and those obtained through displacement-based approaches. In these elements, the degrees of freedom for vertex nodes do not involve curvatures. The establishment of elements is accomplished by approximating the displacement field through piecewise functions.

To build these elements, a complementary energy function was used within the element. In this energy expression, the proper stress function was utilized as a practical capricious. In other words, some elementary systematic answers were allocated for stress purposes. These trial purposes were coordinated with each element's number of degrees of freedom. After some mathematical operations, the element equation was established. To demonstrate the performances of the proposed elements, several benchmarks were analyzed. Comparison studies were performed with two previously offered compatible and displacement-based elements. All numerical solutions showed good results, and could be obtained for the displacements, as well as the stress, by using new elements. While the previous elements could only determine only stress or displacement responses. Both displacement and stress responses could be accurately determined using the proposed elements in this study. It should be emphasized that all four suggested elements led to satisfactory outcomes, and always converged to the exact solutions. In the majority of the analyzed benchmark structures, the KIT and NIT elements were the ones that provided better solutions. This merit was due to the recommended analytical stress functions. Considering the computational costs and the quality of the obtained results, the NIT is the best-suggested element. It is found that if the solutions in highly refined meshes are required, the NIT element takes less time than the KIT element. As a result, the novel presented elements are able to predict the stress and deformation of plates by the average error of 0.21% and 0.42%, respectively, in comparison with the exact answers which highlight and robustness of the presented elements.

Finally, the element proposed in this study has been established based on previous stress functions. So, for further investigations in the future, it is recommended to establish Airy's stress function based on new compatible and incompatible shape functions.

7. References

[1] Sze, K. Y. and Zhu, D. (1998) "A simple assumed strain method for enhancing the accuracy of the cubic triangular C0 plate bending element" Finite Elements in Analysis and Design, Volume 29, Issue 1, Pages 21-33.

[2] Karimi Pour, A. and Noroozinejad Farsangi, E. (2023) "Representing Capabilities of Novel Semi-Analytical Triangular Plate Elements" The Journal of Strain Analysis for Engineering Design.

[3] Karimi Pour, A. and Noroozinejad Farsangi, E. (2023) "Airy Stress Function for Proposed Thermoelastic Triangular Elements" Journal of Engineering Mathematics.

[4] Rezaiee-Pajand, M. and Karimi Pour, A. (2022) "Easy function for solving linear elasticity problem", Structural Engineering and Mechanics, 81, 3, 335-348.

[5] Rezaiee-Pajand, M., Karimi Pour, A. and Attari, M. (2020) "A precise splice length model for reinforced concrete structures", Proceedings of the Institution of Civil Engineers - Structures and Buildings.

[6]   Rezaiee-Pajand, M. and Karimi Pour, A. (2022) "Analytical Scheme for Solid Stress Analysis", International Journal of Applied Mechanics, 12, 6, 2050071.

[7]   Rezaiee-Pajand, M. and Karimi Pour, A. (2022) "Two rectangular elements based on analytical functions", Two rectangular elements based on analytical functions, 5, 2, 147-157.

[8]   Rezaiee-Pajand, M. and Karimi Pour, A. (2022) "Stress Analysis by Two Cuboid Isoparametric Elements", European Journal of Computational Mechanics, 28, 5.

[9]   Rezaiee-Pajand, M. and Karimi Pour, A. (2019) "Three stress-based triangular elements", Engineering with Computers, 36, 4, 1325-1345.

[10]   Öztorun, N. K. (2006) "A rectangular finite element formulation" Finite Elements in Analysis and Design, Volume 42, Issue 12, Pages 1031-1052.

[11]   Esen, I. (2013) "A new finite element for transverse vibration of rectangular thin plates under a moving mass" Finite Elements in Analysis and Design, Volume 66, Pages 26-35

[12]   Haldar, S. and Sheikh, A. H. (2011) "Bending analysis of composite folded plates by finite element method" Finite Elements in Analysis and Design, Volume 47, Issue 4, Pages 477-485

[13]   Wang, K. F. and Wang, B. L. (2013) "A finite element model for the bending and vibration of nanoscale plates with surface effect" Finite Elements in Analysis and Design, Volume 74, Pages 22-29

[14]   Flores, F. G. and Oñate, E. (2011) "Wrinkling and folding analysis of elastic membranes using an enhanced rotation-free thin shell triangular element" Finite Elements in Analysis and Design, Volume 47, Issue 9, Pages 982-990.

[15]   Franciosa, P., Palit, A., Gerbino, S. and Ceglarek, D. (2019) "A novel hybrid shell element formulation (QUAD+ and TRIA+): A benchmarking and comparative study" Finite Elements in Analysis and Design, Volume 166, 103319.

[16]   Duan, J. B., Lei, Y. J. and Li, D. K. (2011) "Fracture analysis of linear viscoelastic materials using triangular enriched crack tip elements" Finite Elements in Analysis and Design, Volume 47, Issue 10, Pages 1157-1168.

[17]   Mu, L. and Zhang, Y. (2020) "Cracking elements method with the 6-node triangular element" Finite Elements in Analysis and Design, Volume 177, 103421.

[18]   Zhuang, X. Y., Huang, R. Q., Zhu, H. H., Askes, H. and Mathisen, K. (2013) "A new and simple locking-free triangular thick plate element using independent shear degrees of freedom" Finite Elements in Analysis and Design, Volume 75, Pages 1-7.

[19]   Ma, X. and Chen, W. (2013) "Refined 18-DOF triangular hybrid stress element for couple stress theory" Finite Elements in Analysis and Design, Volume 75, Pages 8-18

[20]   Zhao, J., Chen, W. and Ji, B. (2010) "A weak continuity condition of FEM for axisymmetric couple stress theory and an 18-DOF triangular axisymmetric element" Finite Elements in Analysis and Design, Volume 46, Issue 8, Pages 632-644.

[21]   Kaveh, A. and Daei, M. (2009) "Efficient force method for the analysis of finite element models comprising of triangular elements using ant colony optimization" Finite Elements in Analysis and Design, Volume 45, Issue 10, Pages 710-720

[22]   Hu, W., Wu, C. T. and Koishi, M. (2012) "A displacement-based non-linear finite element formulation using meshfree-enriched triangular elements for the two-dimensional large deformation analysis of elastomers" Finite Elements in Analysis and Design, Volume 50, Pages 161-172.

[23]   Liu, G. H., Zhang, Q. H. and Sze, K. Y. (2011) "Spherical-wave based triangular finite element models for axial symmetric Helmholtz problems" Finite Elements in Analysis and Design, Volume 47, Issue 4, Pages 342-350.

[24]   Huang, M., Zhao, Z. and Shen, C. (2010) "An effective planar triangular element with drilling rotation" Finite Elements in Analysis and Design, Volume 46, Issue 11, Pages 1031-1036.

[25]   Kaveh, A. and Koohestani, K. (2008) "Efficient finite element analysis by graph-theoretical force method; triangular and rectangular plate bending elements" Finite Elements in Analysis and Design, Volume 44, Issues 9–10, Pages 646-654.

[26]   Chen, J. and Li, C. J. (2019) "A 3D triangular prism spline element using B-net method", European Journal of Mechanics - A/Solids, Volume 75, Pages 485-496

[27]   Cui, X., Duan, S. Y., Huo, S. H. and Liu, G. R. (2021) "A high order cell-based smoothed finite element method using triangular and quadrilateral elements", Engineering Analysis with Boundary Elements, Volume 128, Pages 133-148

[28]   Zander, N., Bériot, H., Hoff, C., Kodl, P. and Demkowicz, L. (2022) "Anisotropic multi-level hp-refinement for quadrilateral and triangular meshes", Finite Elements in Analysis and Design, Volume 203, 103700

[29]   Kamiński, M. (2022) "Uncertainty analysis in solid mechanics with uniform and triangular distributions using stochastic perturbation-based Finite Element Method", Finite Elements in Analysis and Design, Volume 200, 103648

[30]   Cho, J. R. (2022) "Non-linear bending analysis of FG-CNTRC plate resting on the elastic foundation by natural element method", Engineering Analysis with Boundary Elements, Volume 141, Pages 65-74

[31]   de Almeida1, J. P. M., Maunder, E. A. W. and Tiago, C. (2019) "A general degree semi-hybrid triangular compatible finite element formulation for Kirchhoff plates" International Journal of Numerical Methods in Engineering. 00: 1-36.

[32]   Bourdarias, C., Gerbi, S. and Ohayon, J. (2003) "A three-dimensional finite element method for biological active soft" ESAIM: Mathematical Modelling and Numerical Analysis. 37, 4, 725–739

[33]   Fleck, N. A., Muller, G. M., Ashby, M. F. and Hutchinson, J. W. (1994) "Strain gradient plasticity: theory and experiment", Acta Metallurgica et Materiali, 42(2): 475–487.

[34] Fu. X. R., Cen. S, Li. C. F and Chen. X. M. (2008) "Analytical trial function method for the development of new 8-node plane element based on the variational principle containing Airy stress function" Engineering Computations: International Journal for Computer-Aided Engineering and Software Vol. 27 No. 4, 2010 pp. 442-463.

[35] Zienkiewicz, O.C., Taylor, R.L., Papadopoulos, P. and Onates, E. (1990) "Plate bending elements with discrete constraints: new triangular elements" Comparers & Structures, Vol. 35 (4): 505-522.

[36] Shang, Y., Cen, S. and Ouyan, W. (2018) "New hybrid-Trefftz Mindlin-Reissner plate elements for efficiently modeling the edge zones near free/SS1 edges" Engineering Computations, 35 (1).

[37] Sze, K.Y. and Wu. Z.H. (2019) "24 DOFs Four-Node Quadrilateral Elements for Gradient Elasticity" International Journal for Numerical Methods in Engineering, 119 (12).

[38] Fischer, P., Mergheim, J. and Steinmann, P. (2010) "On the C^1 continuous discretization of non-linear gradient elasticity: A comparison of NEM and FEM based on Bernstein–Bezier patches" International Journal for Numerical Methods in Engineering. **82**(8):1282–1307